JOURNAL OF SOLID STATE CHEMISTRY **121,** 87–94 (1996)
ARTICLE NO. 0013

Anionic Polymeric Bonds in Nickel Ditelluride: Crystal Structure, and Experimental and Theoretical Band Structure

W. Bensch and W. Heid

Institut für Anorganische Chemie, Universität Frankfurt, Marie-Curie-Strasse 11, D-60439 Frankfurt-am-Main, Germany

M. Muhler

Fritz-Haber-Institut, Faradayweg 4, D-14195 Berlin, Germany

and

S. Jobic, R. Brec, and J. Rouxel

Laboratoire de Chimie des Solides, Institut des Matériaux de Nantes, 2 rue de la Houssinière, 44072, Nantes Cedex 03, France

Received February 8, 1995; in revised form July 31, 1995; accepted August 3, 1995

Nickel ditelluride was prepared in different ways. Single crystal X-ray investigations reveal that the products are always nonstoichometric with respect to the Ni content. Relatively short intra- and interslab Te–Te contacts are indicative of a polymeric network with multiple Te–Te bonds explaining the very low *c*/*a* value of 1.37 of the hexagonal cell. Experimental valence band spectra (UPS) confirm that $NiTe_2$ is a metal. The emission at the Fermi level E_F is due to Ni *d* and Te *p* states. This assignment is supported by the results of the calculated density of states curve (DOS) which demonstrates that Te *p* states contribute more than 50% to the DOS at E_F. Core level spectra (XPS) give evidence that Ni is in the paramagnetic Ni(II) (d^8) state. The chemical shift of the Te 3*d* core level leads to the assignment of an oxidation state of −1, in good agreement with the oxidation state of about −1.2 deduced from the relation between the Te–Te distances versus oxidation states of the anion in $(Te_2)^{2-}$, Te^{2-}. The three-dimensional character of $NiTe_2$ deduced from the crystal structure is further confirmed by the calculated energy dispersion $E(k)$.

INTRODUCTION

Although the transition metal disulfides and diselenides MX_2 have been studied extensively with respect to their chemical and physical properties, little is known about the tellurides. In previous contributions (1–5) it was demonstrated that the ''classical'' description of the bonding properties of ditellurides of the late transition elements with the CdI_2-type structure corresponding to M^4 $(Te^{2-})_2$ does not adequately illuminate the bonding situation. The formation of three-dimensional pyrite and marcasite structures on the right side of the Periodic Table reflects the destabilization of the higher oxidation states of the cations when going from the left to the right of the Periodic Table. This observation is in line with the successive lowered energy of the *d* electronic band levels, the loss of directionality of the bonds when moving from sulfur to tellurium, and the decrease of electronegativity within the column, which leads to an essentially *sp* valence band higher in energy. The lower *d* levels of the elements on the right side of the Periodic Table and the energetically higher *sp* valence band of tellurium may lead to a *d* cationic/*sp* anionic redox competition, making further studies of the ditellurides of particular interest. The present contribution reports the results of crystal structure investigations, electronic band structure calculations (LMTO and extended Hückel), as well as experimental band structure investigation obtained on nickel ditelluride.

EXPERIMENTAL

A variety of nickel ditelluride samples were prepared in different ways.

Method A. Weighted amounts of the elements with a ratio 1:2 for Ni and Te were placed in evacuated and sealed silica tubes. Prior to their use, the ampoules were dried under vacuum at elevated temperatures to remove the thin water film on their inner wall. The mixture was heated at 975 K for 3 days and afterward cooled to room temperature. After the sample was ground, it was heated at 1065 K for 2 days and at 645 K for 4 days. The product was reground and annealed at 645 K for 2 weeks. Finally, the tube was slowly cooled to room temperature. The prod-

0022-4596/96 $12.00

TABLE 1
Technical Details of Data Collection and Some Refinement Results for Three Different $Ni_{1+x}Te_2$ Samples

	$Ni_{1.027(5)}Te_2$	$Ni_{1.055(2)}Te_2$	$Ni_{1.060(7)}Te_2$
Space group	$P\bar{3}m1$	$P\bar{3}m1$	$P\bar{3}m1$
a(Å)	3.8635(5)	3.8690(3)	3.8659(5)
c(Å)	5.275(2)	5.288(1)	5.292(2)
V(Å^3)	68.19(4)	68.55(2)	68.49(4)
Z	1	1	1
mg	316.4	317.0	317.4
ρ_{calc}(mg/m^3)	7.704	7.667	7.694
μ(mm^{-1})	27.983	27.895	27.974
T(K)	298	298	298
Index ranges	$-1 \le h \le 6$	$-3 \le h \le 5$	$-5 \le h \le 5$
	$-5 \le k \le 6$	$-5 \le k \le 3$	$-5 \le k \le 5$
	$-8 \le l \le 8$	$-8 \le l \le 8$	$0 \le l \le 8$
ΣI	879	599	445
Unique data	181	117	117
$N_o(F_o > 4s(F))$	180	115	115
Min./max. trans.	0.646/0.800	0.590/0.734	0.625/0.962
x^a	0.033(3)	0.029(1)	0.037(4)
y^b	0.000025	0.0000	0.0005
N_p	8	8	8
R(%)	2.17	0.92	2.89
R_w(%)	2.21	0.90	3.23
GOOF	1.39	1.17	1.01
$\Delta F(e^-/Å^3)$	2.67/−3.54	0.97/−0.66	1.22/−2.12

[a] Extinction correction: $F^* = F[1 + 0.002xF^2/\sin(2\Theta)]^{-1/4}$.
[b] Weighting scheme: $w = 1/(\sigma^2(F) + yF^2)$.

uct consisted of silver-gray irregularly shaped crystals and black hexagonal-shaped needles of elemental tellurium.

Method B. To prepare better quality crystals a chemical transport reaction was tested using iodine as transport agent. As a starting material a mixture with an excess of elemental Te (Ni:Te = 1:2.5) was placed in the colder zone (973 K) of a silica tube (length 15 cm), the hotter zone being set at 1020 K. After 8 days irregularly shaped silver-grayish crystals deposited in the ampoule hot zone.

Method C. Crystals of excellent quality were obtained during an attempt to prepare $NiTaTe_5$ at temperatures above those reported in Ref. 6. The nickel ditelluride could be easily identified as silver-gray needle-like crystals.

Out of batches A and B several crystals were tested for single crystal X-ray work before a suitable crystal could be found for structure determination. The peak profiles of the reflections of all other crystals were very broad, indicative of a poor crystalline quality. Intensity data were collected on a STOE AED II diffractometer, using monochromated Mo$K\alpha$ radiation (λ = 0.7107 Å). Oscillation photographs were taken about the different axes. They gave no indications of twinning. Technical details on the data acquisition as well as some refinement results are summarized in Table 1. The observed intensities were reduced to F_0. Lorentz, polarization, and a numerical absorption correction were applied. The final weighting scheme was varied until no significant dependence on F/F_{max} or $\sin\theta/\lambda$ was observed. All calculations were done with the software package SHELXTL plus. Atomic coordinates and the equivalent displacement parameter as well as the anisotropic displacement parameters are listed in Table 2 and selected interatomic distances are given in Table 3.

The band structure of $NiTe_2$ has been calculated, assuming charge self-consistency, by means of the linear muffin tin orbital (LMTO) method (7) in the ASA mode. Exchange and correlation have been treated within the framework of local density functional theory using the parametrization of Hedin and Lundqvist. Relativistic effects have been accounted for by using the so-called scalar–relativistic approximation, ignoring the influence of spin–orbit coupling. For the basis functions a maximum angular momentum of $l_{max} = 2$ has been used for all components. The results presented here have been obtained by using the tetrahedron method, performing the necessary Brillouin zone (BZ) integration with 1080 k-points during the SCF cycle. Important numerical results are listed in Table 4.

X-ray photoelectron spectroscopy (XPS, Mg$K\alpha$ = 1253.6 eV) and ultraviolet photoelectron spectroscopy (UPS, He I = 21.2 eV and He II = 40.8 eV) investigations were performed in a Leybold–Heraeus ultrahigh vacuum (UHV) environment. The analyzer was operated in the constant pass energy mode. The resolution of the XPS spectra was 1.3 eV for all samples. For UPS the resolution was better than 100 meV. The base pressure was always better than 3×10^{-10} mbar. The energy scale was calibrated using Au $4f_{7/2}$ = 84.0 eV. The sample was ground in UHV until a clean oxygen-free surface was obtained. After subtraction of the satellites and correction of the background using a Shirley background, the composition of the sample

TABLE 2
Atomic Coordinates and Equivalent Isotropic Displacement Coefficients U_{eq} (Å^2), Occupation Ratios and Anisotropic Displacement Parameters for $Ni_{1.055(2)}Te_2$

	x	y	z	U_{eq}	t
Ni(1)	0	0	0	0.010(1)	1.
Te	1/3	2/3	−0.2508(1)	0.011(1)	1.
Ni(2)	0	0	1/2	0.010(2)	0.055(2)
	U_{11}	U_{33}			
Ni(1)	0.0102(2)	0.0111(2)			
Te	0.0114(2)	0.0116(1)			

Note. $U_{22} = U_{11}$; $U_{12} = \frac{1}{2}U_{11}$; $U_{13} = U_{23} = 0$. Equivalent isotropic U defined as one-third of the trace of the orthogonalized U_{ij} tensor. The anisotropic displacement factor takes the form: $-2\pi^2(h^2a^{*2}U_{11} + \cdots + 2\,hka^*b^*U_{12})$.

TABLE 3
Bond Lengths (Å) for $Ni_{1.055(2)}Te_2$

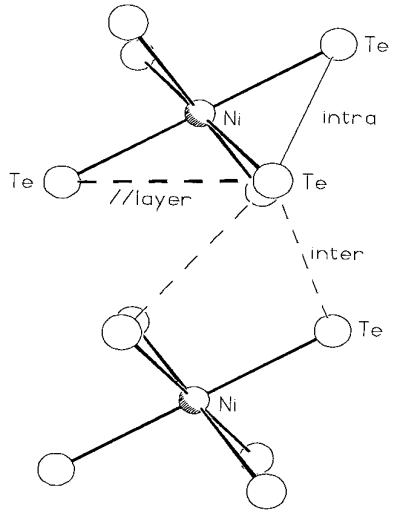

Ni(1)–Te	2.598(1)	Ni(2)–Te	2.644(1)
$Te–Te_{intra}$	3.468(1)[a]	$Te–Te\|\|_{layer}$	3.8690(3)[a]
$Te–Te_{inter}$	3.455(1)[a]		

[a] ‖Layer, parallel to ($NiTe_2$) sandwich; intra, intra-sandwich; and inter, inter-sandwiches.

was calculated with the empirical cross sections given by Briggs and Seah (8) and was found to be in good agreement with the nominal composition.

RESULTS AND DISCUSSION

The Crystal Structure

In a previous contribution the existence of stoichiometric nickel ditelluride was questioned due to the fact that the unit cell volume of "$NiTe_2$" reported in the literature is nearly identical to that of $CoTe_{1.7}$ (1). Our experiments confirm these doubts but the deviation from the stoichiometric composition is only small.

As mentioned under Experimental we successfully selected three different crystals for the three different preparation methods. In all cases the difference Fourier syntheses calculated with stoichiometric $NiTe_2$ (Ni and Te refined anisotropically) showed the highest residual peaks in the van der Waals gaps between the Te layers. It was therefore assumed that excess Ni atoms occupy part of the octahedral holes in these gaps in a statistical way. The site occupation factor was determined by fixing the isotropic displacement parameter of the excess Ni (Ni(2)) at a value identical with that obtained for the Ni atom in the $NiTe_2$ layers (Ni(1)). At the same time the site occupation factor was refined. This procedure led to $Ni_{1.027(5)}Te_2$ (Method B), $Ni_{1.055(2)}Te_2$ (Method C), and $Ni_{1.060(7)}Te_2$ (Method A). In the final refinement cycles the Ni(2) atom was refined with a fixed site occupation factor and a freely varying isotropic displacement parameter.

The slightly poorer R values obtained for $Ni_{1.027(5)}$ and $Ni_{1.060(7)}$ may be the result of an inappropriate absorption correction due to the irregular shape of the crystals. As mentioned under Experimental oscillation photographs of the different crystals gave no indication of twinning. Hence we exclude twinning as the reason for the somewhat poorer R values.

The possibility of a Frenkel defect equilibrium with interstitial Ni atoms and vacancies in the full layers cannot be excluded. A small deviation from a full occupation of the Ni(1) site is difficult to detect by X-ray diffraction. But to achieve stoichiometry via Frenkel defects about 5% of the Ni atoms in the full layers must reside on interstitial sites, an anomalously high percentage.

The smallest deviation from stoichiometry was observed for the crystal selected from the product of the chemical transport reaction which was conducted with a large excess of tellurium. Lattice parameters as well as c/a ratios for different nickel ditellurides are presented in Table 5. As can be seen, the values reported are somewhat at variance,

TABLE 4
Lattice Parameters and Numerical Results of the Band Structure Calculations for $NiTe_2$

	$NiTe_2$
a	3.869
c	5.288
S_{Te}	1.879
S_{Ni}	1.459
Q_{Te}	−0.023
Q_{Ni}	0.046
$n_{Te,s}(E_F)$	0.018
$n_{Te,p}(E_F)$	0.256
$n_{Te,d}(E_F)$	0.070
$n_{Te}(E_F)$	0.344
$n_{Ni,s}(E_F)$	0.016
$n_{Ni,p}(E_F)$	0.061
$n_{Ni,d}(E_F)$	0.428
$n_{Ni}(E_F)$	0.505
$n_{tot}(E_F)$	1.192

Note. The lattice parameters a and c as well as the Wigner Seitz radii S are given in Å, and Q stands for the atomic charge. The component and angular momentum resolved DOS at the Fermi level n_α, $l(E_F)$ is given as states/eV · atom while the total DOS is given per FU.

TABLE 5
Lattice Constants and *c/a* Ratio for $NiTe_2$ Taken from the Literature

	a	*c*	*c/a*	Ref.
$NiTe_2$	3.855	5.256	1.363	1
$Ni_{1.05}Te_2$	3.879	5.300	1.370	29
$NiTe_2$	3.835	5.250	1.371	29
$NiTe_2$	3.8542	5.2604	1.365	39
$NiTe_2$	3.8547	5.2610	1.365	40
$Ni_{1.053}Te_2$	3.8605	5.2784	1.367	40
$Ni_{1.026}Te_2$	3.8567	5.2690	1.366	40
$NiTe_{2.05}$	3.8547	5.2605	1.365	40
$Ni_{1.027(5)}Te_2$	3.8635(5)	5.275(2)	1.365	This work
$Ni_{1.055(2)}Te_2$	3.8690(3)	5.288(1)	1.367	This work
$Ni_{1.060(7)}Te_2$	3.8659(5)	5.292(2)	1.369	This work

even for "stoichiometric" $NiTe_2$ and for tellurides with a similar composition. These differences may be due to the fact that most of the crystal structure determinations were performed using the multiple Weissenberg method, and hence the data are less accurate than those obtained during the present study.

Because there are only minute differences between the crystal structures of the three samples, the following discussion is valid for all three samples. Using charge balance arguments and with the usual configuration, $NiTe_2$ must be formulated as $Ni^4(Te^{2-})_2$ with an unexpectedly high oxidation state for a telluride compound. At first, the results of crystal structure refinement suggest that $NiTe_2$ belongs to the CdI_2-type structure. But a detailed analysis of the interatomic Te–Te separations reveals that the Te–Te parallel to the layers as well as the interlayer distances of 3.468(1) and 3.455(1) Å, respectively, are significantly shorter than the sum of two Te^{2-} ionic radii ($r(Te^{2-})$ = 2.11 Å (9)). It is also to be noted that these interatomic distances are larger than Te_2 pair-containing phases (2.763 Å in $HfTe_5$ (10) and 2.793 Å in $ZrTe_3$ (11). Actually, the short Te–Te separations found in $NiTe_2$ are comparable to the values reported for other ditellurides of the late transition elements (1), values which are indicative of Te–Te bonds. Because the Te atoms are not only bonded through the van der Waals gaps but also through the structure slabs the small value for the *c*-axis as well as the low *c/a* ratio is easily understood. A probably nonbonding separation between the anions is found at 3.869 Å (not too far from the Te ··· Te distances across the van der Waals gap observed in $HfTe_2$ and $ZrTe_2$ (1)). This analysis strongly suggests that $NiTe_2$ is not a layered phase but a three-dimensional phase. This assumption is supported by the fact that the anisotropic displacement components U_{11} and U_{33} of Ni(1) and Te are nearly identical (compare Table 2).

To further support the assumption of a three-dimensional material, tight-binding band structure calculations (12) were carried out using an extended Hückel type Hamiltonian (13). A modified Wolfsberg–Helmolz formula was used to calculate the nondiagonal $H\mu\nu$ values (14). The ionization potentials (eV) and exponents used were (15, 16) −20.78 and 2.51 for Te 5*s*, −13.20 and 2.16 for Te 5*p*, −9.70 and 2.10 for Ni 4*s*, −5.15 and 2.10 for Ni 4*p*. Double ζ orbitals were used for Ni 3*d*. The ionization potential exponents and contraction coefficients were −13.49, 5.75, 2.30, 0.57979, and 0.57819, respectively. A 150 *k*-point set for the density of states calculation was chosen according to the geometrical method of Ramirez and Böhm (17). Calculated overlap population at the Fermi level (which is not identical to the bond order but which scales it) for the three different Te ··· Te contacts (3.468(1), 3.455(1), and 3.8690(3) Å) are +0.04, +0.07, and −0.01, respectively. Thus bonding Te ··· Te interactions do exist between tellurium atoms of two different layers. Hence $NiTe_2$ belongs to the subgroup of the CdI_2-type which was classified as the polymeric CdI_2-type (1).

In $IrTe_2$, with an iridium cation III, the Te–Te interlayer and through-slab distances correspond well to an oxidation state of −1.5 for Te (1). Because these distances are shorter in $NiTe_2$ we may conclude that the oxidation state should lie between −1 and −1.5. This conclusion is supported by electronic band structure investigations (see below).

THE EXPERIMENTAL BAND STRUCTURE

The Valence Band Region

The valence band spectra of $NiTe_2$ recorded with He I, He II, and XPS are displayed in Fig. 1. The height of the emission intensity at E_F convincingly reveals that $NiTe_2$ is a metal. Two relatively well-resolved peaks are located

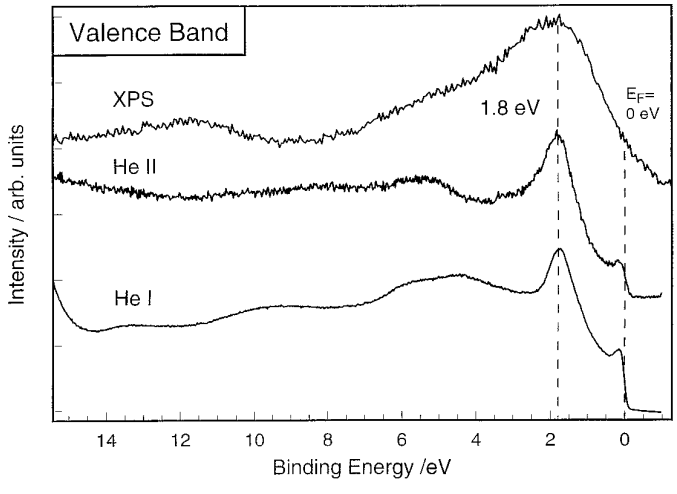

FIG. 1. The valence band region of $NiTe_2$ recorded with He I, He II, and Mg$K\alpha$ (XPS) radiations.

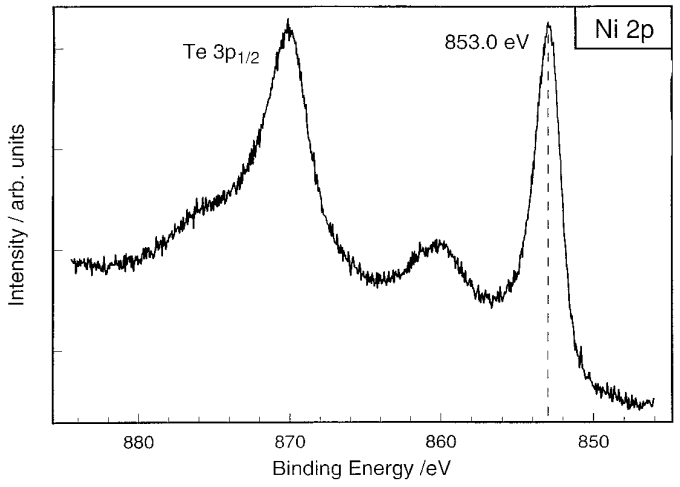

FIG. 2. The Ni 2*p* core level region of $NiTe_2$. Note the satellite structure located at about 860 eV.

directly below E_F and at 1.8 eV below E_F, respectively. The differences between the He I, He II, and XPS spectra are due to the different cross sections for the excitation energies of He I, He II, and Mg$K\alpha$. In addition, the resolution of the XPS spectrum is too low to reproduce the features observed in the He UP spectra. Using the cross sections for the different excitation energies given by Yeh and Lindau (18) (He I: Te 5*p*: 4.758, Ni 3*d*: 3.984; He II: Te 5*p*: 0.5043, Ni 3*d*: 7.877), a qualitative assignment of the different emissions seems to be possible. The height of the emission at the Fermi level is significantly lower for He II than for He I. If the emission at E_F is only due to Ni 3*d* states it should be larger for the He II radiation. On the other hand, if the emission is only caused by Te 5*p* states the height should be reduced by roughly a factor of 9. From the observed difference in the height of the emission for the He II and He I radiations and taking into account the tabulated cross sections, one can assume that Te 5*p* and Ni 3*d* states both contribute to the emission at E_F. The peak at about 1.8 eV below the Fermi level is mainly due to Ni 3*d* states. It is to be noted that a similar peak located at nearly the same binding energy was observed for NiS in the paramagnetic state (19). In the monosulfide the Ni 3*d* band extends from 0 to 3 eV below E_F.

Between 2.5 and 7 eV below E_F a broad and nearly featureless valence band is observed. It can be assumed that the broad emission at about 4 eV below E_F is due to Ni *d* and Te *p* hybridized states.

The Ni 2p Core Level Region

The Ni 2*p* core level region is displayed in Fig. 2. The intense peak at about 871 eV is due to the Te $3p_{1/2}$ core level. The shoulder on the high binding energy (b.e.) side is caused by the Ni $2p_{1/2}$ level. The evaluated b.e. for the Ni $2p_{3/2}$ level of 853 eV is only about 0.27–0.5 eV larger than the values reported for elemental Ni (20–22). But it is significantly lower than the b.e.'s given for Ni(II) oxides (854.4–856.0 eV) or Ni(II) halides (855.3–856.7 eV). Data for Ni(II) containing chalcogenides are rare. For NiS the b.e. ranges from 852.8 to 853.2 eV (23, 24) and for NiSe only one value of 853.2 eV was reported (25). The disulfide exhibits a slightly higher b.e. of 853.6 eV and the b.e. for $NiSe_2$ was reported to be 853.2 eV (26). But it must be noted that the disulfide, as well as the diselenide, crystallizes in the pyrite structure type with X_2^{2-} anions, giving rise to the oxidation state of II for Ni. The broad emission centered at about 860 eV is due to a shake-up satellite caused by final state effects. This is a highly interesting observation because a similar shake-up satellite structure was observed for the monosulfide NiS (27) as well as for NiS_2 and $NiSe_2$ (25) in which Ni is in the oxidation state II. On the other hand no shake-up satellites are generally observed for diamagnetic low-spin Ni^2 (d^8) compounds (28). Because $NiTe_2$ was reported to be a weak paramagnet (10, 29) the occurrence of this shake-up satellite structure gives evidence for Ni in the d^8 state.

The Te 3d Core Level Region

The Te 3*d* core level region is displayed in Fig. 3. The evaluated b.e. of the Te $3d_{5/2}$ core level of 572.3 eV is smaller than the values given for elemental Te (572.98 and 572.85 eV (30, 31); average, 572.9 eV using 18 data; range, 572.1 to 573.54 eV), but it is significantly lower than in Te halides or oxides (575.8–576.9 eV (32, 33)). Compared with the b.e. published for the ditellurides $IrTe_2$ or Ir_3Te_8 (573.0 and 573.5 eV (1)) and $NbTe_4$ (572.8 eV (34)) the value obtained for $NiTe_2$ is lower and can better be com-

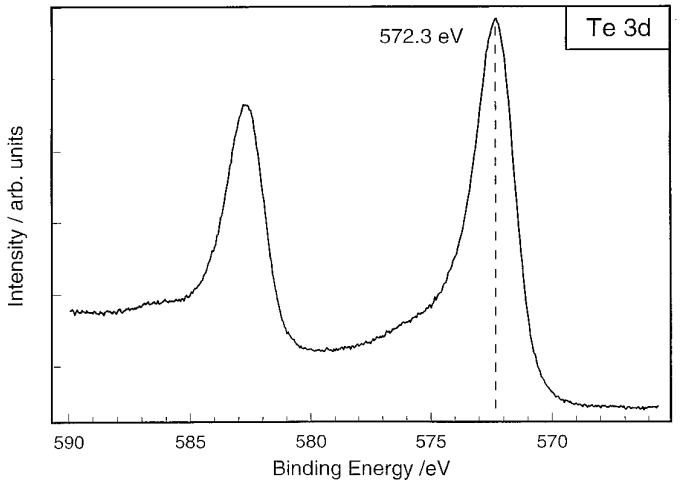

FIG. 3. The Te 3*d* core level spectrum of $NiTe_2$.

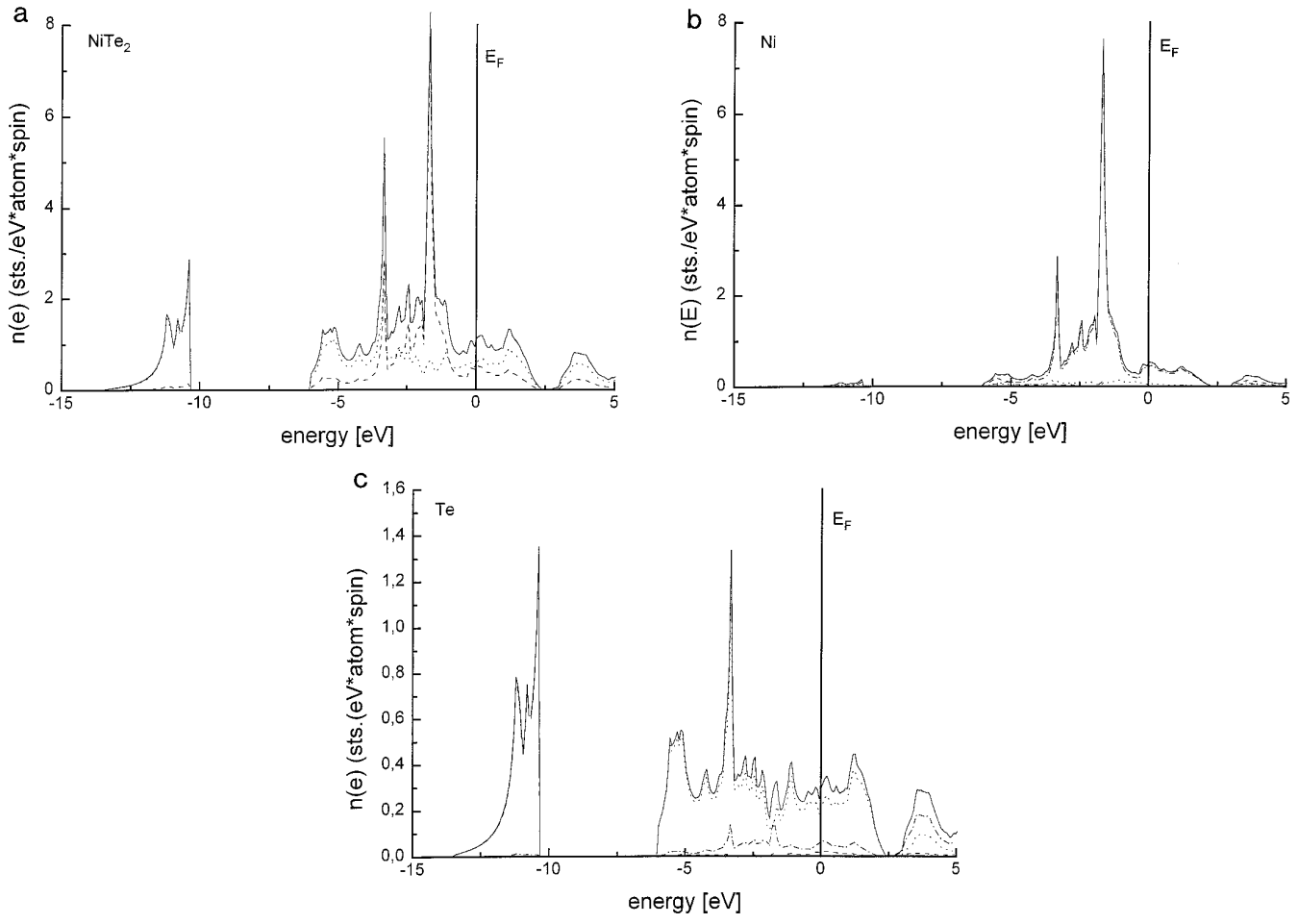

FIG. 4. Total, component, and angular momentum resolved density of states of $NiTe_2$. The panel a gives the total DOS (full line) together with the Ni (---) and Te ($\cdots$) contributions. The panels b and c give the angular momentum resolved DOS of Ni and Te. The *s*, *p*, and *d* contributions are represented by the lines ---, $\cdots$ and -·-·-, respectively, while the full line gives the sum of these parts.

pared with the b.e.'s reported for monotellurides (ZrSiTe, 572.5 eV (35); CdTe, 572.47 eV (36)).

In general, the b.e.'s listed in the NIST XPS database for the different tellurium compounds scatter by about ± 0.5 eV for the same compound. A rough estimate of the b.e.'s versus the oxidation state yields a chemical shift of the Te $3d_{5/2}$ core level line of about 0.6 eV per oxidation number. The average b.e. of the $3d_{5/2}$ emission for elemental Te is found to be 572.9 eV. Hence, a shift of 0.6 eV relative to elemental Te and the assumption of a linear relationship between chemical shift and oxidation number would lead to the assignment of Te^{-1} in $NiTe_2$. Using the relation between the Te–Te distances versus oxidation states of the anion in $(Te_2)^{2-}$, Te^{2-} (1) an oxidation state of about -1.2 of the tellurium in $NiTe_2$ would be deduced.

The Te 3*d* peaks exhibit a pronounced tail on the high b.e. side. Such highly asymmetric core level lines are observed for the Cu 2*p* core level as well as for the S 2*p* peaks of binary Cu sulfides and selenides (37, 38), which are metals. This asymmetry was attributed to the coupling of the core hole with the delocalized electron density located near the Fermi level. Because the ditelluride is a metal and Te states contribute significantly to the density of states at the Fermi level this final state effect may be the reason for the asymmetric lineshape of the Te 3*d* core levels.

THE THEORETICAL BAND STRUCTURE

The calculated total density of states curve (DOS) as well as the contributions of the two elements to the DOS are shown in Figs. 4a–4c. The most important numerical results and lattice parameters are summarized in Table 4. As Fig. 4 shows the Te 5*s* states give rise to a narrow valence band at a binding energy of 10–14 eV with only weak hybridization with Ni states. On the other hand the valence band between -6 and -1.5 eV has contributions from Ni and Te with dominating Ni 3*d* states. Between

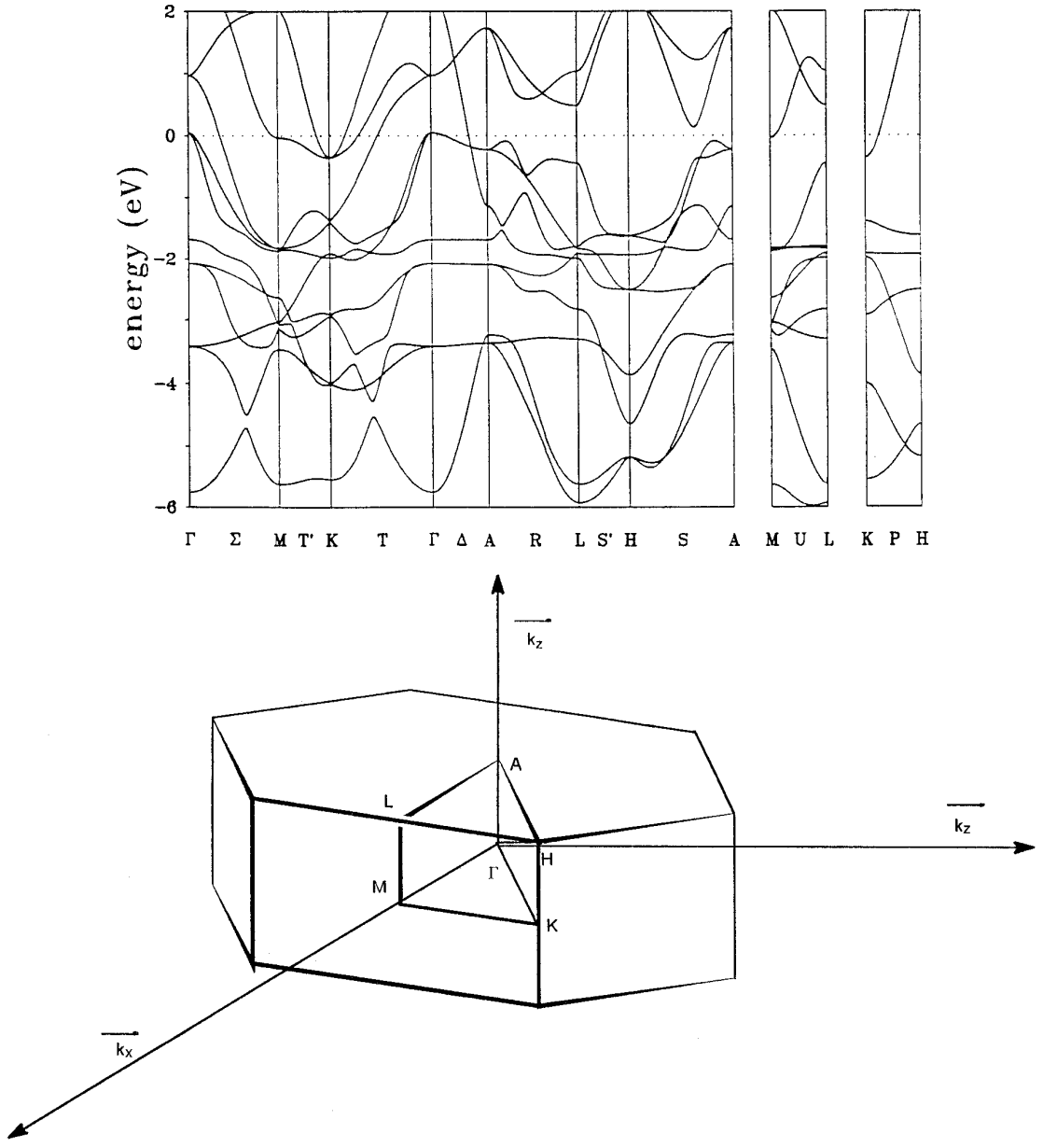

FIG. 5. The dispersion relations $E(k)$ for $NiTe_2$ (top). The special symmetry points of the hexagonal Brillouin zone (bottom).

the Fermi level and about −1.5 eV a not-well-pronounced minimum in the DOS curve is observed. Above this dip the DOS increases again, giving rise to a value of 1.192 states/eV · FU at the Fermi level (FU = formula unit). As can be seen from Fig. 4 and Table 4 the contributions coming from Te *p* states dominate (60%) here while Ni states contribute only 40% to the DOS. This applies not only to the states at the Fermi level but more or less to the whole conduction band ranging from −0.5 eV to around 2.5 eV. It is quite interesting to note that for Te the *d*-like character contributes about 20% to the component projected DOS (behavior that cannot be understood on the basis of a simple tight-binding description, ignoring *d*-valence states for this element). It must be noted here that the interpretation of the experimental valence band spectra given above is in full agreement with the calculated density of states curve.

Together with the component and angular momentum resolved DOS a rather detailed insight into the anisotropy of the chemical bonding is supplied by the dispersion relation $E(k)$ shown in Fig. 5. As can be seen, the Fermi level crosses at least four conduction bands within the basal plane in the directions (Γ–*M*–*K*–Γ). These bands exhibit in part a large dispersion, indicative of strong bonding

interactions between the different atoms in that plane. The Fermi level also crosses at least one conduction band in directions perpendicular to the basal plane (Γ–A, M–L, K–H). This band shows a high dispersion, indicative of relatively strong bonding interactions perpendicular to the layers.

In summary, the results of the electronic band structure calculations reveal that $NiTe_2$ is an anisotropic material with strong bonds within the layers and weaker bonds perpendicular to the layers. Therefore, $NiTe_2$ can be viewed as a true three-dimensional material rather than a ''classical'' layer compound with the charge balance $Ni^{2}Te_2^{1-}$. To further confirm the three-dimensional nature of $NiTe_2$ electrical conductivity measurements should be performed. Unfortunately, the crystals obtained so far were too small and showed a very anisotropic shape.

ACKNOWLEDGMENTS

Financial support by the Deutsche Forschungsgemeinschaft (DFG) as well as by the Fonds der Chemischen Industrie is gratefully acknowledged.

REFERENCES

1. S. Jobic, R. Brec, and J. Rouxel, *J. Solid State Chem.* **96,** 169 (1992).
2. L. Monconduit, M. Evain, F. Boucher, R. Brec, and J. Rouxel, *Z. Anorg. Allg. Chem.* **616,** 177 (1992).
3. S. Jobic, M. Evain, R. Brec, P. Deniard, A. Jouanneaux, and J. Rouxel, *J. Solid State Chem.* **95,** 319 (1991).
4. E. Canadell, S. Jobic, R. Brec, and J. Rouxel, *J. Solid State Chem.* **98,** 59 (1992).
5. E. Canadell, S. Jobic, R. Brec, J. Rouxel, and M.-H. Whangbo, *J. Solid State Chem.* **99,** 189 (1992).
6. E. W. Liimatta and J. A. Ibers, *J. Solid State Chem.* **78,** 7 (1989).
7. H. L. Skriver, ''The LMTO Method.'' Springer, Berlin, 1983.
8. D. Briggs and M. P. Seah, ''Practical Surface Analysis,'' 2nd ed., Vol. 1. Wiley, New York, 1983.
9. R. D. Shannon, *Acta Crystallogr. Sect. A* **32,** 751 (1976).
10. S. Furuseth, L. Brattas, and A. Kjekshus, *Acta Chem. Scand.* **27,** 2367 (1973).
11. S. Furuseth and H. Fjellvag, *Acta Chem. Scand.* **45,** 694 (1991).
12. M.-H. Whangbo and R. Hoffmann, *J. Am. Chem. Soc.* **100,** 6093 (1978).
13. R. Hoffmann, *J. Chem. Phys.* **39,** 1397 (1963).
14. J. H. Ammeter, H. B. Bürgi, J. Thibeault, and R. Hoffmann, *J. Am. Chem. Soc.* **100,** 3686 (1978).
15. E. Canadell, Y. M. Athey, and M.-H. Whangbo, *J. Am. Chem. Soc.* **110,** 104 (1988).
16. E. Canadell and M.-H. Whangbo, *Inorg. Chem.* **26,** 3974 (1987).
17. R. Ramirez and M. C. Böhm, *Int. J. Quantum Chem.* **30,** 391 (1986).
18. J. J. Yeh and I. Lindau, *At. Data Nucl. Data Tables* **32,** 1 (1985).
19. A. Fujimori, M. Matoba, S. Anzai, K. Terakura, M. Taniguchi, S. Ogawa, and S. Suga, *J. Magn. Magn. Mater.* **70,** 67 (1987).
20. C. P. Li, A. Proctor, and D. M. Hercules, *Appl. Spectrosc.* **38,** 880 (1984).
21. J. C. Klein and D. M. Hercules, *J. Catal.* **82,** 424 (1983).
22. C. R. Anderson, R. N. Lee, J. F. Morar, and R. L. Park, *J. Vac. Sci. Technol.* **20,** 617 (1982).
23. R. B. Shalvoy and P. J. Reucroft, *J. Vac. Sci. Technol.* **16,** 567 (1979).
24. T. Dickinson, A. F. Povey and P. M. A. Sherwood, *J. Chem. Soc. Faraday Trans. I* **73,** 332 (1977).
25. A. B. Mandale, S. Badrinarayanan, S. K. Date, and A. P. B. Sinha, *J. Electron. Spectrosc. Relat. Phenom.* **33,** 61 (1984).
26. H. Van der Heide, R. Hemmel, C. F. van Bruggen, and C. Haas, *J. Solid State Chem.* **33,** 17 (1980).
27. S. Hüfner, T. Riesterer, and F. Hulliger, *Solid State Commun.* **54,** 689 (1985).
28. L. Yin, I. Adler, T. Tsang, L. J. Matienzo, and S. O. Grim, *Chem. Phys. Lett.* **24,** 81 (1974).
29. W. Klemm and N. Fratini, *Z. Anorg. Allg. Chem.* **251,** 222 (1943).
30. R. Nyholm and N. Martensson, *J. Phys. C.* **13,** L279 (1980).
31. E. Laine, M. Tamminen, R. Makela, and M. Pessa, *J. Mater. Sci.* **18,** 295 (1983).
32. M. K. Bahl, R. L. Watson, and K. J. Irgolic, *J. Phys. Chem.* **66,** 5526 (1977).
33. A. J. Ricco, H. S. White, and M. S. Wrighton, *J. Vac. Sci. Technol. A* **2,** 910 (1984).
34. M. K. Bahl, *J. Phys. Chem. Solids* **36,** 485 (1975).
35. M. Muhler, W. Bensch, O. Helmer, M. Knecht, and H. Ebert, *J. Phys. Chem.,* **99,** 3326 (1996).
36. H. S. White, A. J. Ricco, and M. S. Wrighton, *J. Phys. Chem.* **87,** 5140 (1983).
37. J. C. W. Folmer and F. Jellinek, *J. Less-Common Met.* **76,** 153 (1980).
38. J. C. W. Folmer and D. K. G. DeBoer, *Solid State Commun.* **38,** 1135 (1981).
39. S. Furuseth, K. Selte, and A. Kjekshus, *Acta Chem. Scand.* **19,** 257 (1965).
40. J. Barstad, F. Gronvold, E. Rost, and E. Vestersjo, *Acta Chem. Scand.* **20,** 2865 (1966).